

Revisiting the formation history of the minor-axis dust lane galaxy NGC1947

M. Spavone^{1,2*}, E. Iodice², R. Calvi¹, D. Bettoni³, G. Galletta⁴, G. Longo^{1,2},
P. Mazzei³, G. Minervini¹

¹*Dipartimento di Scienze Fisiche, Università Federico II, via Cinthia 6, I-80126 Napoli, Italy*

²*INAF-Astronomical Observatory of Naples, via Moiariello 16, I-80131 Napoli, Italy*

³*INAF-Astronomical Observatory of Padova, Vicolo dell'Osservatorio 5, 35122 Padova, Italy*

⁴*Dipartimento di Astronomia, Università di Padova, Vicolo dell'Osservatorio 2, 35122 Padova, Italy*

Accepted 2008 November 10 Received 2008 November 05; in original form 2008 July 29

ABSTRACT

In this paper we present a detailed study of the peculiar early-type galaxy NGC1947. The main goal of this work is to constrain the dynamical status and the formation history of NGC1947 by comparing the observed properties with the predictions derived from different galaxy formation scenarios. To this aim, we derived the photometric and kinematical properties of NGC1947. Due to the presence of an extended dust-lane, which crosses the galaxy center along the photometric minor axis, we used near-infrared images (J and K bands) to derive an accurate analysis of the stellar light distribution. Optical images (in the V and R bands) are used to derive the color profiles and color maps to study the structure of the dust-lane. The observed kinematics confirm the presence of two components with decoupled angular momentum: gas and dust rotate along the minor axis, while the rotation velocities of the stars are observed along the major axis. The complex structure observed in NGC1947 support the hypothesis that some kind of interactions happened in the evolution of this object. We analyzed two alternatives: a merging process and an accretion event. We discussed how the observed properties strongly suggest that the decoupled ring of gas and dust have been accreted from outside.

Key words: galaxies: individual – galaxies: formation – galaxies: evolution – galaxies: interactions.

1 INTRODUCTION

One of the major open issues in modern cosmology is to understand how galaxies formed and evolved. It is likely that the formation of galaxies is dominated by two processes: the assembly of luminous and dark matter through accretion and mergers, and the conversion of baryonic and non-baryonic matter into stars. The Cold Dark Matter (CDM) scenario for galaxy formation is based on the hierarchical mass assembly (Cole et al. 2000) which predicts that the observed galaxies and their dark halo were formed through a repeated merging process of smaller systems. This is the reason why the study of galaxy interactions and merging has received an ever increasing attention in recent years, both on the observational and theoretical sides.

It has been shown that gravitational interactions and mergers affect the morphology and dynamics of galaxies from the Local Group to the high-redshift universe (e.g. Conselice et al. 2003; Bundy et al. 2004; Lin et al. 2004; Kartaltepe et al. 2007; De Propris et al. 2007; Lotz et al. 2008). These observational results support the scenario in which the merging of two disk galaxies produces spheroidal merger remnants with physical characteristics, such as density profiles, mean velocity dispersion and surface brightness, quite similar to those observed for E and S0s (Toomre & Toomre 1972; Barnes & Hernquist 1992; Bekki 1998a; Bournaud et al. 2005). However, other types of interactions, such as smooth accretion and stripping seem to be equally important in the growth of galaxies and the relative weights of the various processes depends on the environment, which drive many morphological features observed in galaxies, such as bars, shells (see Malin & Carter 1980) and highly inclined or even counter-rotating rings/disks (see Galletta 1996 for a review). Concerning the latter morphology, different degrees of evolution of these peculiar rings/disks are seen: some cases the decoupled matter is composed by stars and gas, and regions of recent star formation are also observed (Iodice et al. 2002, Iodice et al. 2002; Reshetnikov et al. 2005); other cases show rings with a particularly smooth structure (Iodice et al. 2004), or formed only by gas (Bettoni et al. 2001). In general, these peculiar galaxies have very large amount of gas (Richter et al. 1994 and Galletta et al. 1997) and dust which lies in the same plane of the decoupled ring/disk (e.g. Arnaboldi et al. 1997; Bettoni et al. 2001; van Driel et al. 2002; Cox et al. 2006). The decoupling of the angular momentum between the two components cannot be explained by the collapse of a single protogalactic cloud, thus a “second event” must have happened in

the formation history of these systems. Given all the above, such peculiar galaxies turn out to be the ideal laboratory where to derive detailed information about many of the physical processes controlling galaxy interactions and merging.

Several theoretical works based on numerical simulations, have tested two plausible scenarios for the origin of the decoupled matter: either gas accretion from infall processes, or merging between gas-rich galaxies (Thakar & Ryden 1996, Thakar & Ryden 1998; Reshetnikov & Sotnikova 1997; Bekki 1998b; Bournaud & Combes 2003, Bournaud et al. 2005). In both cases, the decoupled material forms a ring (Quinn 1991, Hernquist & Weil 1993) which after a while settles into one of the principal planes of the gravitational potential associated with the host galaxy (Heisler et al. 1982; Bertola et al. 1991; Bournaud & Combes 2003). Multiple accretion events may also account for more complicated objects, like NGC2685 where two orthogonal rings are observed around the main galaxy body (Schinnerer & Scoville 2002; Bournaud & Combes 2003).

The unequal-mass merging of two disk galaxies is the other way to build a galaxy with an highly inclined ring/disk: the morphology and kinematics of the merger remnants depends on the initial orbital parameters and the initial mass ratio of the two galaxies involved in the process (e.g. Bournaud & Combes 2003, Bournaud et al. 2005).

External gas can also be accreted from cosmic web filaments with high inclined angular momentum relative to the main disk plane (Davé et al. 2001; Semelin & Combes 2005; Macciò et al. 2005) and recent theoretical work has argued that this might even be the most realistic way by which galaxies get their gas (Kereš et al. 2005). Finally, in the standard CDM scenario, recent high-resolution cosmological simulations of galaxy formation have shown that angular momentum misalignment during the hierarchical structure formation can also lead to the formation of highly inclined ring/disk (Brook et al. 2008).

Although most of the formation scenarios proposed so far seem able to account for many of the observed morphologies and kinematics for this class of peculiar galaxies, the relative weight of the two main processes, i.e. the merging of two galaxies or external gas accretion, remains still uncertain. The reasons for such an uncertainty mainly reside in the poor understanding of many processes which are at work during gravitational interactions such as, for instance, gas dissipation, star formation efficiency, feedback, gas re-heating, etc., phenomena that all strongly affect the dynamical history of galaxies. Detailed photometric and kinematical observations of systems in different dynamical states, both in the local universe and at higher redshift, can help better constraining the physics of such processes. To this aim, we

present a detailed study of the peculiar early-type galaxy NGC1947, that can be considered as a prototype of minor-axis dust-lane galaxy (see Fig.1). In 1978 Bertola & Galletta (1978) made the first study of a small sample of peculiar galaxies (including NGC1947) that all showed a dust-lane crossing perpedicularly the central spheroidal body: the similarities in observed properties let them to conclude that, by a morphological point of view, these objects should be considered as a new class of galaxies. A larger sample of dust-lane galaxies, including objects similar to NGC1947, have been studied by Hawarden et al. (1981), and they found that galaxies with a minor axis dust-lane form a dominant group among all dust-lane galaxies. The difference of the angular momenta of the stellar, gaseous and dusty components is a clear proof that the three components have not all the same origin, and an accretion of new material from outside was addressed as possible formation mechanism for such class of objects (Hawarden et al. 1981).

This work is a part of an ongoing research project aimed to select a sample of peculiar and interacting galaxies, for which both multiwavelength photometric and kinematical data are available, and to compare the observed properties with the predictions derived from different galaxy formation scenarios.

The main properties of NGC1947 are listed in Tab.1. The morphological classification of this galaxy is somewhat controversial. In fact, NGC1947 was initially classified as S0 peculiar by de Vaucouleurs et al. (1976) and $S0_3$ peculiar by Sandage & Tammann (1987) while, due to the absence of a photometrically detectable disk, Bertola et al. (1992) and Oosterloo et al. (2002) classified it as an E1 crossed by a series of dust lanes along the optical minor axis. As shown by Bertola et al. (1992) the peculiarity of NGC1947 resides in the presence of three parallel minor-axis dust lanes, which appear as concentric rings, in addition to the central one, which is typical of the dust-lane galaxies. The main dust lane crosses the center along the SW direction, while the others, less pronounced and parallel to the central one, are detected in the NE side. The galaxy also exhibits a ring of molecular gas (Sage & Galletta 1993) and a disk-like distribution of ionized gas centered on the nucleus and at the same position angle of the dust lane. Moreover, the stars in NGC1947 rotate along the galaxy's major axis, perpendicular to the gas rotation axis (Bertola et al. 1992). A considerable amount of HI was detected by Oosterloo et al. (2002): the HI gas is distributed in a warped disk, which is aligned with the dust lane and it rotates in the same sense; the HI mass is about $3.4 \times 10^8 M_{\odot}$.

This paper is structured as follows: in Section 2 we describe the observations and data

Table 1. General properties of NGC1947

Parameter	Value	Ref.
Morphological type	S0 peculiar	NED ^a
R.A. (J2000)	05h26m47.6s	NED
Dec. (J2000)	-63d45m36s	NED
Helio. Radial Velocity	1100 km/s	NED
Redshift	0.0037	NED
Distance	15 Mpc	
Axial ratio _K	0.98	
$(J - K)_T$	0.931	2MASS ^b
Total m _J (mag)	8.445 ± 0.02	2MASS
Total m _K (mag)	7.510 ± 0.03	2MASS
$M(HI)(M_{\odot})$	3.4×10^8	Oosterloo et al. (2002)
$M_{dust}(M_{\odot})$	15.3×10^5	Oosterloo et al. (2002)
$L_K(L_{\odot})$	2.65×10^{11}	
$M/L_K(M_{\odot}/L_{\odot})$	0.2	

^a NASA/IPAC Extragalactic Database

^b 2 Micron All Sky Survey

reduction procedures. The morphology in the NIR and optical bands and the light and color distribution of the galaxy are described in Section 3, while in Section 3.1 we present a 2-dimensional model of the light distribution. In Section 4 we discuss the star and gas kinematics along the two principal photometric axes of the galaxy, and in Section 14 is presented and discussed the spectral energy distribution derived for NGC1947. Finally, in Section 5 we draw our conclusions.

Throughout this paper we shall adopt for NGC1947 a distance of about 15 Mpc based on $H_0 = 75 \text{ km s}^{-1} \text{ Mpc}^{-1}$ and an heliocentric radial velocity $V = 1100 \text{ km s}^{-1}$, which implies that 1 arcsec = 0.07 kpc.

2 OBSERVATIONS AND DATA REDUCTION

Near-Infrared data - NGC1947 belongs to a selected sample of peculiar galaxies observed (December 2002) in the Near-Infrared (NIR) J and K bands with the SofI infrared camera at the ESO-NTT telescope. The field of view was $4.92 \times 4.92 \text{ arcmin}^2$ with a pixel scale of 0.292 arcsec/pixel. Images were acquired in the offsetting mode: a cycle was defined by several images on the target, interspersed with sky frames and with an integration time of 60 seconds; each object frame was taken with a small offset from the galaxy center and the sky frames were taken before and after each galaxy frame. More cycles were obtained in the K band than in the J band, in order to have a better estimate of the background level. A

total exposure time of 720 sec was obtained on the target in the J band and of 2760 sec in the K band. The average seeing during the observing time is about $FWHM \simeq 1.1$ arcsec.

The data reduction was carried out using the CCDRED package in the IRAF¹ (*Image Reduction and Analysis Facility*) environment. The main strategy adopted for each dataset included dark subtraction², flatfielding correction, sky subtraction and rejection of bad pixels. Finally, all frames were registered and co-added to form the final science frames. Several standard stars, from Persson et al. (1998), observed at the beginning, middle and end of each observing night, were used to transform instrumental magnitudes into the standard J and K band systems.

The calibrated K band image of NGC1947 is shown in Fig. 2 (right panel).

Optical data - CCD images of NGC1947 in the Johnson V and R bands were extracted from the European Southern Observatory (ESO) Public Archive. They had been obtained with the red arm of EMMI at ESO-NTT telescope and the detector used for the observations consisted of two MIT/LL CCDs, with a scale of 0.332 arcsec/pixel (with a 2×2 binning) and a field of view of 22.7×22.7 arcmin². The average seeing was $FWHM \sim 0.99 \pm 0.03$ arcsec for the V band, and $FWHM \sim 0.94 \pm 0.03$ for the R band. There were seven exposures available in the V band with an integration time of 100s, and five exposures in the R band with an integration time of 60s. The raw frames were pre-processed using the standard IRAF tasks for de-biasing and flat-fielding. The flat-field was performed using normalized sky flat. Each CCD was reduced independently: the images were dithered and shifted in order to obtain a complete image of both the galaxy and its surroundings. The frames of each CCDs were combined, after de-biasing and flat-fielding, to filter out cosmic ray hits. Finally, we used the IRAF task IRMOSAIC to obtain a mosaic of the images. Multiple exposures of identical fields were aligned using several stars present in the images and then co-added to produce a final median averaged image. An average value of the background emission was estimated in several regions of the sky far from the galaxy light.

In order to perform the photometric calibration, several Landolt standard stars were observed in the same bands.

The final, calibrated V band image of NGC1947 is shown in Fig. 2 (left panel).

Spectroscopic data - The spectroscopic data were extracted from the European Southern

¹ IRAF is distributed by the National Optical Astronomy Observatories, which is operated by the Associated Universities for Research in Astronomy, Inc. under cooperative agreement with the National Science Foundation.

² Bias frame is included in the Dark frame.

Observatory (ESO) public archive³. They have been obtained with the EMMI spectrograph at ESO-NTT in the RILD mode. The data, consisting of four set of spectra, were acquired with a slit $1.0''$ wide, using the GR#5 grism with a dispersion of 5.5 nm mm^{-1} , corresponding to $0.83 \text{ \AA pxl}^{-1}$, in the $380 - 700 \text{ nm}$ wavelength range. The spectra were acquired along both the photometric major ($P.A. = 40^\circ$) and minor ($P.A. = 130^\circ$) axis of NGC1947. The total integration time of both spectra is 600 s; the average seeing turned out to be $FWHM = 1$ arcsec. A set of spectra of standard template *K0III* stars were also acquired with the same configuration.

Individual frames were pre-reduced using the standard IRAF image processing package; the wavelength calibration was made using the IRAF TWODSPEC.LONGSLIT package and a set of He-Ar-Ne lamp spectra taken for each observing night. Sky subtraction was performed with the IRAF BACKGROUND package, by using a narrow region at both edges of the slit where the galaxy contamination is minimum. Finally, all the exposures for both axis were co-added in the final median averaged 2D spectra, which were used to derive the central velocity dispersion and the rotation curve along both axes. The velocity dispersion and the radial velocity were derived with the Fourier Quotient Technique (Sargent et al. 1977; Bertola et al. 1984), using the standard stars as templates. One of the main source of statistical and systematics errors is the template mismatching; so we performed tests to verify if the standard star we used to derive the kinematics of the galaxy was the best one. These tests showed no template mismatching. In both spectra some extended emission lines are well visible, in particular [OIII] $\lambda 5007\text{\AA}$, H_α , [NII] $\lambda\lambda 6548, 6583$ and [SII] $\lambda\lambda 6717, 6731$. These lines allowed us to measure the gas rotation curves also. To measure the rotation curves, every record of each galaxy spectrum was fitted with a Gaussian function on the emission line using the task SPLOT of IRAF package. The H_α line was not measured due to the presence of a strong absorption component, for this reason only the more extended [NII] $\lambda 6583$ line with a signal to noise ratio ≥ 2 was fitted. Taking into account the average seeing and the EMMI pixel scale, the final stellar and gaseous rotation curves were derived by adopting a binning factor of 3 along the spatial direction to obtain independent data points. They will be presented in Fig.12 and described in the sec.4. Due to the low signal-to-noise ratio (which is about 20 in the center and decreases to about 10 towards the outer regions), the kinematic profiles are about 4 times less extended than the light profiles (Fig.3).

³ <http://archive.eso.org/>

3 PHOTOMETRY: MORPHOLOGY, LIGHT AND COLOR DISTRIBUTION

The most prominent feature of NGC1947 is the extended dust-lane, which crosses the galaxy center along the photometric minor axis. Since the dust optical depth decreases toward longer wavelengths, NIR photometry is necessary to reduce as much as possible the dust absorption, that strongly affects the starlight distribution in the galaxy. Thus, we used near-infrared images (J and K bands) to easily identify the inner structures of NGC1947 and accurately analyse the stellar light distribution. On the other hand, optical images (in the V and R bands) are used to derive the optical versus NIR color profiles and color maps to study the structure of the dust-lane.

Isophote analysis - We used the IRAF-ELLIPSE task on the NIR images to perform the isophotal analysis for NGC1947 and the results are shown in Fig.3. The average surface brightness extends up to about 80 arcsec from the galaxy center (see Fig.3); in the K band, the half-light radius is $R_e = 24.4 \pm 2$ arcsec $\sim 1.86 \pm 0.15$ kpc. For a semi-major axis r , in the range $10 \leq r \leq 40$ arcsec, the ellipticity and P.A. are almost constant and equal to 0.05 and 40° , respectively, that indicates that in this regions the isophotes are almost round and co-axial. For $r \leq 20$ arcsec the dust lane perturbs the ellipticity and P.A. profiles and also the shape parameters a_4/a , which are shown in Fig.3. This effect is even more evident in the J than in the K band. For $10 \leq r \leq 25$ arcsec, the shape parameters are all consistent with zero, thus the isophotes do not significantly deviate from purely elliptical shape, while at larger distances (out to ~ 40 arcsec) they tend to be more disk-like (see Fig.3). In Tab.2 we give the integrated magnitudes and average colors within two circular apertures, derived for the NIR J and K bands, and optical V and R bands. The apertures were chosen in order to make the comparison easier with the magnitudes of NED.

Light and color distribution - In Fig.4 we show the light profiles along the major ($P.A. = 40^\circ$) and minor ($P.A. = 130^\circ$) axis in the NIR and in the optical bands respectively. The light distributions in the optical V and R bands are very much perturbed by the presence of the dust-lane, in the regions between 10 and 30 arcsec on the NE side of the major axis, and for $r < 20$ arcsec on the SE side of the minor axis. Except for this, neither NIR nor optical profiles show any significant feature.

We have derived the $V - R$ (Fig.5), $J - K$ (Fig.7, left panels) and $V - K$ (Fig.6, left panels) color profiles along both photometric axes of NGC1947, and the 2-dimensional $V - K$ and

$J-K$ color maps (Fig.6 and Fig.7 right panels, respectively). On average, the central regions of the galaxy have redder colors, with a maximum value of $V-R = 1.05$, $J-K = 1.5$ and $V-K = 5$. At larger radii the colors are bluer. In all color profiles, on the NE side of the major axis, between 10 to 30 arcsec, double red peaks are observed, at $r=18$ arcsec and $r=30$ arcsec where $V-R=0.85$ and $V-K=4$: such features are due to the ring-like structure of the dust-lane, already suggested by Bertola et al. (1992) and described in Sec.1, which stands out very clearly in the 2-dimensional V-K color map (Fig.6). The dust-lane perturbs only the SE side of the minor axis color profile, within 10 arcsec from the center: this suggests that the dust-lane is slightly misaligned with respect to the photometric minor axis. This is also confirmed by the 2-dimensional J-K color map (see Fig.7, right panel): with respect to the nucleus, which is very red, there are two “thin” and redder structures which do not lie on the same direction. In particular, the one on the NW side is on a parallel direction towards North. The full extension of the inner dust-lane is about 27 arcsec.

Stellar population ages - We derived the integrated V-K and J-K colors in two circular apertures: one including the nuclear regions of the galaxy inside a radius of 1 kpc $\sim 0.54R_e$, where $V-K = 3.2$ and $J-K = 1.02$, and one out to $1.5R_e \sim 2.85$ kpc, where $V-K = 2.84$ and $J-K = 0.99$. The stellar population synthesis model by Bruzual & Charlot (2003) were used to reproduce the integrated colors in these regions, in order to derive an estimate of the stellar population ages. We adopted a star formation history with an exponentially decreasing rate, that produces a reasonable fit of the photometric properties of early-type galaxies in the local Universe. It has the following analytical expression: $SFR(t) = \frac{1}{\tau} \exp(-t/\tau)$, where the τ parameter quantifies the “time scale” when the star formation was most efficient. Adopting $\tau = 1$ Gyr, the correspondent evolutionary tracks were derived for both solar metallicity, $Z = 0.02$, and for a higher value, $Z = 0.05$; both values were assumed constant with age. In every model it has been assumed that stars form according to the Salpeter (1955) IMF, in the range from 0.1 to $125M_\odot$. To account for the V-K and J-K colors the best model is that obtained for $Z = 0.05$, from which we derived an age of about 3.9 Gyrs for the inner region and of about 2.3 Gyrs for the outer one. These estimates have to be considered as an upper limit to the last burst of star formation. These constraints will turn to be fundamental in the discussion on the formation scenarios (Sec.5).

3.1 2-Dimensional model of the light distribution

We performed a 2-dimensional model of the light distribution in the K band, where the effect of dust absorption is weaker, and stars are accurately masked. To this aim, we used the GALFIT task (Peng et al. 2002). As a first attempt and according to the morphological classification given for NGC1947 in the previous work (see Tab.1) as an Elliptical, the galaxy light is modelled through a single Sersic law (Sersic 1968): the fit is very poor, suggesting the presence of an additional component in the outer regions. Therefore, we adopted a double-component model as the superposition of a Sersic law (Sersic 1968) plus an exponential profile (Freeman 1970). The fit improves considerably; the fitted light profiles for the major and minor axis of NGC1947 are shown in Fig.8 and Fig.9. The structural parameters derived from the fit are: the bulge total magnitude $m_b = 17.7 \pm 0.01 \text{ mag}$, the bulge scale length $r_e = 74.0 \pm 0.7 \text{ arcsec}$, the disk total magnitude $m_d = 17.0 \pm 0.02 \text{ mag}$, the disk scale length $r_h = 121.1 \pm 0.3 \text{ arcsec}$ and the Sersic exponent $n = 2.83 \pm 0.01$, leading to a **bulge total luminosity-to-disk total luminosity ratio**, $L_B/L_D \simeq 0.43$.

Along both axes, inside a 30 arcsec radius from the galaxy center, the residuals reflect the presence of the dust-lane, which is more pronounced along the NE region of the major axis, where the galaxy appears to be less luminous than the model. Such an effect is much more clear in the residual image (see Fig.10) obtained by subtracting the 2D model to the galaxy. In order to analyze the structure of the dust-lane in NGC1947, we used the 2D model obtained in the K band, which is less perturbed by dust absorption, to match the light distribution in the V band. To this aim, the V band image of NGC1947 was scaled to the K band, by accounting for the average V-K color (see Sec.3). In the residuals (Fig.11) two main features stand out very clearly: *i*) the concentric ring-like structure of the dust-lane, superposed to *ii*) a bright region (within 20 arcsec from the center) which is more luminous on the SW side with respect to the NE side. The existence of such luminous "counterpart" is reliable due to the fit interpolation, which is an average of the whole galaxy light (see Fig.8 and Fig.9): this is also confirmed by the absence in the V-K color profile (see Fig.6) of any bluer component on the SW region, which should have appeared in the V-band residual image respect to the K band one. By this analysis, we estimate that the dust-lane extends by 49.6 arcsec from SE to NW, with a thickness of about 23 arcsec.

Table 2. Magnitudes and Colors for NGC1947 in circular aperture.

aperture radius (arcsec)	m_J ± 0.05	m_K ± 0.04	m_V ± 0.01	m_R ± 0.01	J-K ± 0.09	V-R
15.7	10.44	9.35	13.20	11.81	1.09	1.39
81.2	8.91	7.90	11.26	9.99	1.01	1.27

4 STELLAR AND GASEOUS KINEMATICS ALONG THE PRINCIPAL PHOTOMETRIC AXES OF NGC 1947

Major axis - The stellar kinematics is more extended on the SW side with respect to the NE and it is measured out to $20'' \sim 1.4$ kpc (Fig. 12, bottom panel), which corresponds to a surface brightness of ~ 21.7 mag arcsec $^{-2}$ in the V band. The rotation curve is not symmetric with respect to the galaxy center: in the range $2'' < r < 14''$ NE, rotation increases, up to a maximum value between 55 and 80 km/s, to be compared with the corresponding distance range on the SW side, where almost no rotation is measured. The kinematics along NE side, for $r > 6''$, is strongly perturbed by the dust-lane, as suggested by the V-K color profiles (Fig.6).

The velocity dispersion remains almost constant within the uncertainties at an average value of $\sim 133 \pm 31$ km/s, out to 10 arcsec from the center. Both the rotation velocity profile and the average velocity dispersion turns out to be consistent with those published by Bertola et al. (1992).

The gas component too shows some rotation along this direction, and the rotation curve has the same extension as the stellar rotation curves (see Fig. 12): it shows a very steep inner gradient, reaching a maximum velocity of ~ 100 km/s on the NE side and ~ 80 km/s on SW side, between $2''$ and $4''$ from the center. Velocities remain almost on these values up to the last measured point. These data (both for emission and absorption) are consistent with, and extend those of Moellenhoff (1982). However, the measured rotation for the gas was not so evident in the data of Moellenhoff (1982).

Minor axis - The stellar kinematics is measured out to the same distance from the galaxy center, i.e. $20''$ (Fig. 12, top panel). On average, stars do not rotate and the velocity dispersion has the mean weighted value of $\sim 146 \pm 37$ km/s within $5''$ from the center.

The gas rotation curve is more extended (up to about $30''$) and better resolved with respect to the stellar rotation curves. Along the major axis, the gas shows a very steep inner gradient, reaching a maximum velocity of ~ 200 km/s between $10''$ and $20''$ from the center. The full extension of the gas rotation curve is of about 60 arcsec, which is about 2 times wider than

the dust-lane (see Sec. 3).

The gas velocity curve presented in this work, even though more extended on the SE side, is consistent with the one published by Moellenhoff (1982).

The observed kinematics led us to conclude that the minor axis is the principal rotation plane of the gaseous disk. Moreover, for this component some rotation is observed even in the direction of the major axis: this implies that the disk is warping towards the inner regions (Arnaboldi & Galletta 1993) and suggests that this component has not reached a stable configuration yet. The average velocity dispersion turns out to be consistent also with values derived by Carollo et al. (1993), according to the kinematics derived along two intermediate directions.

In Fig. 13 we show the stellar and gaseous rotation curves along the minor axis of NGC1947 superposed on the position-velocity plot along the $P.A. = 127^\circ$ of the HI distribution presented by Oosterloo et al. (2002). The HI distribution is more extended than the stellar rotation curve: the HI extends out to about 90 arcsec, while the stellar rotation curve extends up to about 20 arcsec. The HI and gas in the dust-lane rotates in the same sense and with the same amplitude (see Fig.13): this confirms that the HI is in a warped rotating disk associated with the dust-lane, as already suggested by Oosterloo et al. (2002).

5 DISCUSSION AND CONCLUSIONS

In the present work we performed a detailed analysis of the structure of the minor-axis dust-lane galaxy NGC1947, and in what follows we will discuss the implications of our findings on the formation and evolution history of this peculiar object. In particular, we will discuss how the observed properties for NGC1947 presented in this work, compare with the predictions from different formation scenarios for such kind of systems. The main observed properties for NGC1947 that the most likely formation scenario has to account for are *i)* the high-inclined ring of gas and dust which rotates in the perpendicular direction with respect to the stars in the major axes of the S0-like host galaxy, and *ii)* the photometry and kinematics observed for the two decoupled components (stars and gas), in particular, the warp observed for the gas towards the inner regions (sec. 4), which suggests that the inner rings of gas has not settled yet in the equilibrium plane; *iii)* the estimated timescale of the formation mechanism has to be consistent with the age estimates of the different stellar populations.

The presence of two components with different angular momenta, gas and dust along the

minor axis and stars along the major axis, suggests that NGC1947 could not be the result of a single protogalactic cloud collapse and that it may have experienced an interaction event. In this framework, the possible formation scenarios which may account for a galaxy with high inclined ring/disk of gas, stars and dust (discussed in the Sec.1) are *i*) the tidal accretion of gas by outside, and *ii*) the unequal-mass merging of two disk galaxies. In the following we will discriminate between these two scenarios for NGC1947. Furthermore, we will discuss how Smoothed Particles Hydrodynamic (SPH) simulations of isolated collapsing triaxial systems, presented by Mazzei & Curir (2003), may account for peculiar galaxies like NGC1947.

- *Tidal accretion* -

The features observed in NGC1947 lead to the possibility of considering the galaxy as a tidal accretion remnant. The tidal accretion scenario accounts for a large variety of polar structures; many simulations show that the accretion produces warped rings and transient features (see Bournaud & Combes 2003), with processes similar to those leading to the formation of Polar Ring Galaxies (PRGs). Differently from PRGs, in the polar ring of NGC1947 there are not detected stars associated to the gas and dust. Such Interstellar Medium (ISM) could be accreted by a gas-rich donor galaxy during a close passage of a pre-existing S0 galaxy near this companion galaxy. In order to consider the accretion hypothesis, we studied the field around NGC1947 (shown in Fig.15) to see if there are any objects from which the galaxy could have accreted material: inside a radius of about 5 times the diameter of the galaxy, which correspond to about 16 arcmin, (as suggested by Brocca et al. 1997) there is the early-type spiral galaxy ESO 085-GA088, which is at the same redshift of NGC1947, with a radial velocity of 1164 km/s. As discussed by Oosterloo et al. (2002), NGC1947 shows a warped HI disk at the same position angle as the dust lane, while the HI emission of ESO 085-GA088 extends in a direction perpendicular to that of NGC1947: this is the orbital configuration needed to form a polar ring (of gas) through an accretion event (Bournaud & Combes 2003). These observed features may suggest that the donor galaxy could be ESO 085-GA088: in fact, taking into account the linear relative distance of about $16' \sim 70$ kpc, and the relative velocities of the two systems, we estimate the time at which the interaction happened, to be about 1 Gyr ago. Such value estimated in the case of a parabolic orbit has to be considered a lower limit. In the case of a parabolic orbit a longer time is expected, which should be consistent with the upper limit to the last burst of star formation in NGC1947 (estimated in Sec. 3).

- *Merging* -

Unequal-mass merging of two disk galaxies may build a spheroidal galaxy with an high inclined ring/disk of gas, stars and dust. In order to test such formation mechanism, we will compare the observed properties with those expected from simulations performed by Bournaud et al. (2005). To do so, we computed the following quantities:

- the fitted light profile for this galaxy is consistent with a Sersic plus exponential luminosity profile, with bulge/disk=0.43 and bulge/total=0.57 (see Sec.3);
- according to Bournaud et al. (2005), we evaluated the isophotal shape parameters of the galaxy, in the range $[0.55R_{25th}, R_{25th}]$, which is the range between the bulge and the disk optical radius. In this range the ellipticity is almost constant, ~ 0.11 , and the $a_4 \simeq -0.004$ suggests a bulge with a moderate boxiness;
- we have taken into account the global kinematical properties of NGC1947 by deriving the v/σ ratio along the major axis: in the range $[0.55R_{25th}, R_{25th}]$ $v/\sigma \sim 0.15$, while the ratio v_{max}/σ_0 is about 0.62.

Such quantities have been compared with those predicted by numerical simulations for galaxy mergers with various mass ratios (see Tab.2 in Bournaud et al. 2005): we found that they turn to be consistent with those expected for a merging with initial mass ratios 3:1 or 4:1 (Bournaud et al. 2005). This is a mass ratio for which Bournaud et al. 2005 found stable and long lived polar or high-inclined rings of gas, returning to the galaxy along tidal tails, and equatorial rings, that appears as "dust lanes" when they are seen edge-on. Such unequal-mass merger has been proven to be the most likely scenario for another peculiar galaxy: the double-ring ESO 474-G26 (Reshetnikov et al. 2005).

In the hypothesis that NGC1947 may be the result of a merging event, we compare the observed properties of NGC1947 with those of the galaxies that have certainly experienced a merging, such as the galaxies belonging to the Toomre Sequence (hereafter TS, Toomre 1977).

The first step was to place NGC1947 on the TS, to determine at which merger state we are looking at. To this aim, we studied the position of NGC1947 on the plot of the total K band magnitude versus the magnitude within a radius of 1 kpc for the galaxies belonging to the TS, performed by Rossa et al. (2007) (see Fig.25 in that paper). Thus, for NGC1947 we estimated the total K band magnitude and the V, J and K magnitudes within a radius of 1kpc, which are respectively $M_K = -23.3$ mag, $m_V = 12.37$ mag, $m_J = 9.79$ mag and

$m_K = 8.74$ mag. The nucleus of NGC1947 lies in the region between the nuclei of the late-stage mergers and the normal early-type galaxies. This leads to the reasonable conclusion that NGC1947 could be considered a very late-stage merger remnant. As a second step, we compared the V-K and J-K nuclei colors obtained by Rossa et al. (2007) for the galaxies belonging to the TS with those derived for NGC1947 (see Sec.3), by classifying it as late-stage merger (Fig.16 and 17). The J-K colors for NGC1947 are consistent with those of TS galaxies, while in the V-K color plot NGC1947 turns to be bluer relative to the TS galaxies: since no clumps of star forming galaxies are observed in NGC1947, this difference could reasonably be due to the presence of a larger amount of dust in the TS galaxies.

- Formation of NGC1947 through SPH simulations -

We derive a suitable match of the dynamical and photometric properties of NGC1947 with a SPH simulation: Mazzei & Curir (2003) implemented SPH simulations with chemo-photometric evolutionary population synthesis models providing the SED from ultraviolet to near-IR wavelengths. The simulation includes self-gravity of gas, stars and dark matter (DM), radiative cooling, hydrodynamical pressure, shock heating, artificial viscosity, star formation and feedback from evolved stars and type II SNe, as described in Mazzei & Curir (2003). The starting point is a triaxial collapsing system initially composed of 30000 particles, 15000 of gas and 15000 of DM with a relative mass ratio of 0.01. The total mass, M , of the collapsing system is $10^{13}M_{\odot}$. The system is built up as described by Mazzei & Curir (2003), i.e., with a spin parameter, λ , given by $|\mathbf{J}||E|^{0.5}/(GM^{0.5})$, where E is the total energy, J the total angular momentum and G the gravitational constant, equal to 0.06, and it is aligned with the shorter principal axis of the DM halo. It is also assumed a triaxiality ratio of the DM halo, $\tau = (a^2 - b^2)/(a^2 - c^2) = 0.84$, where $a > b > c$, which corresponds to an average radius of about 1 Mpc. Under these conditions, as found out by Mazzei & Curir (2003), the morphology of the resulting galaxy is highly related to the initial properties of the halo, which drive the galaxy formation and evolution. In particular, the dynamical timescales of stars and gas are quite different and, as a consequence, the two components become decoupled during the evolution of the system.

Here, we present the synthetic SED which accounts for chemical evolution, stellar emission, internal extinction and re-emission by dust in a self-consistent way, as described in (Mazzei et al. 1992, 1995). This allows us to extend the SED over four orders of magnitude in wavelength, i.e., from 0.1 to 1000 μm . So the model self-consistently provides morphological, dynamic and chemo-photometric evolution. Fig. 14 compares the predicted SED with

the available data for NGC1947. Such a model suggests that star formation started about 14.5 Gyrs ago, and that the maximum was reached about 9 Gyrs ago. The average age for the inner stellar generations is dated at about 3 Gyrs: this could be due to the still efficient inflow of the gas and is consistent with the findings by Serra et al. (2007), which included such a galaxy in the sample of centrally-rejuvenated objects.

Dynamical predictions of such SPH simulations agree with kinematical features observed for NGC1947 (see Sec. 4): in particular, the model predicts a maximum rotation velocity of about 20 km/s for the stars and of 120 km/s for the gas, and a velocity dispersion in the central regions of about 130 km/s.

- *Conclusions* -

Putting all the above evidences together, we now try to address which are the observational aspects that can help to disentangle in a non ambiguous way the possible formation scenarios for NGC1947 discussed above.

We have found that an unequal-mass merging of two disk galaxies, with a mass ratio in the range 3:1 - 4:1, could account for the average structure and kinematics observed for NGC1947. But this scenario fails to reconcile *i*) the epoch of the merging event with the estimates of stellar population ages in NGC1947; and *ii*) the gas kinematics. According to the simulations (Bournaud et al. 2005), after 3 Gyrs from the merging event, the outer regions of the remnant are characterized by typical signs of the past interaction, like tidal tails and/or shells. Such features are not observed in NGC1947. To account for this, the merger would have occurred very long ago (~ 10 Gyrs) and the ring should be very long-lived: these predictions are not consistent with both *i*) the upper limit to the epoch at which the interaction happened for NGC1947, i.e. ~ 3 Gyrs (see Sec.3) and *ii*) the warped structure of the ring, which suggests that the polar component has not reached a stable configuration yet (see sec.4). Therefore, we can reasonably rule out the merging scenario for the formation of NGC1947 and we can regard the recent polar accretion from a gas rich donor galaxy as one of the most probable interaction event in the formation history of this galaxy.

We have also discussed how such a peculiar object may be the result of processes of galaxy formation and evolution under particular initial conditions, linked to the ratio between baryonic and dark matter: the SPH simulations by Mazzei & Curir (2003) can reasonably account for the observed photometry and kinematics of the galaxy. We aim to further investigate in detail such aspect by comparing the predictions of such a model and observations, but



Figure 1. Color composite image of NGC1947 assembled from EMMI-NTT images in the V (blue channel), J (green channel) and K (red channel) bands. The North is up, while the East is on the left of the image.

they are beyond the aims of the present work and they will be the subject of a forthcoming paper.

ACKNOWLEDGMENTS

The authors wish to thank the anonymous referee whose comments and suggestions greatly improved the presentation of this work. The authors are very grateful to F. Bournaud for many useful discussions and suggestions. E.I. wish to thank E. Pompei for the support given during the data acquisition. This work is based on observations made with ESO Telescopes at the Paranal Observatories under programme ID $< 70.B - 0253(A) >$ and $< 74.B - 0626(A) >$.

REFERENCES

- Arnaboldi M., Galletta G., 1993, *A&A*, 268, 411
- Arnaboldi M., Oosterloo T., Combes F., Freeman K. C., Koribalski B., 1997, *AJ*, 113, 585
- Barnes J. E., Hernquist L., 1992, *ARA&A*, 30, 705
- Bekki K., 1998a, *ApJ*, 499, 635

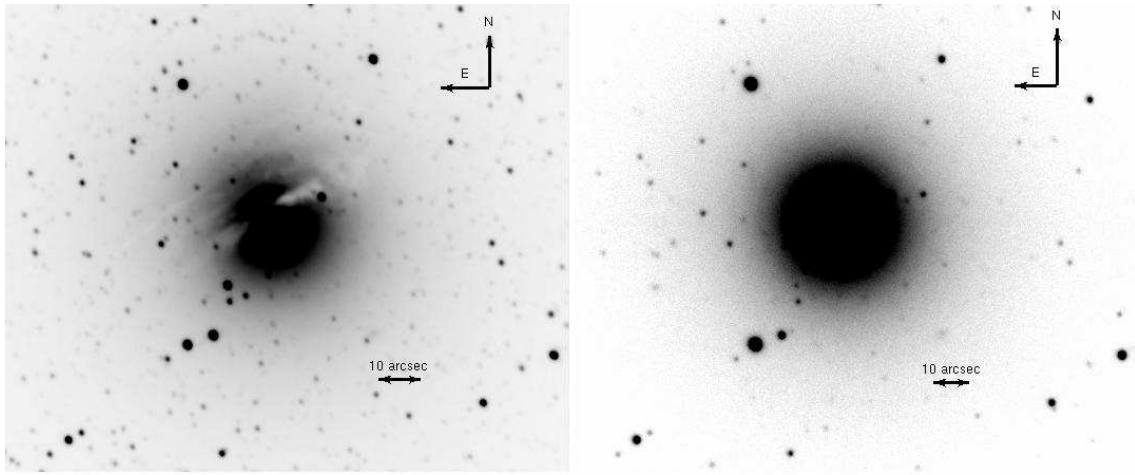


Figure 2. Calibrated K (right panel) and V (left panel) images of NGC1947

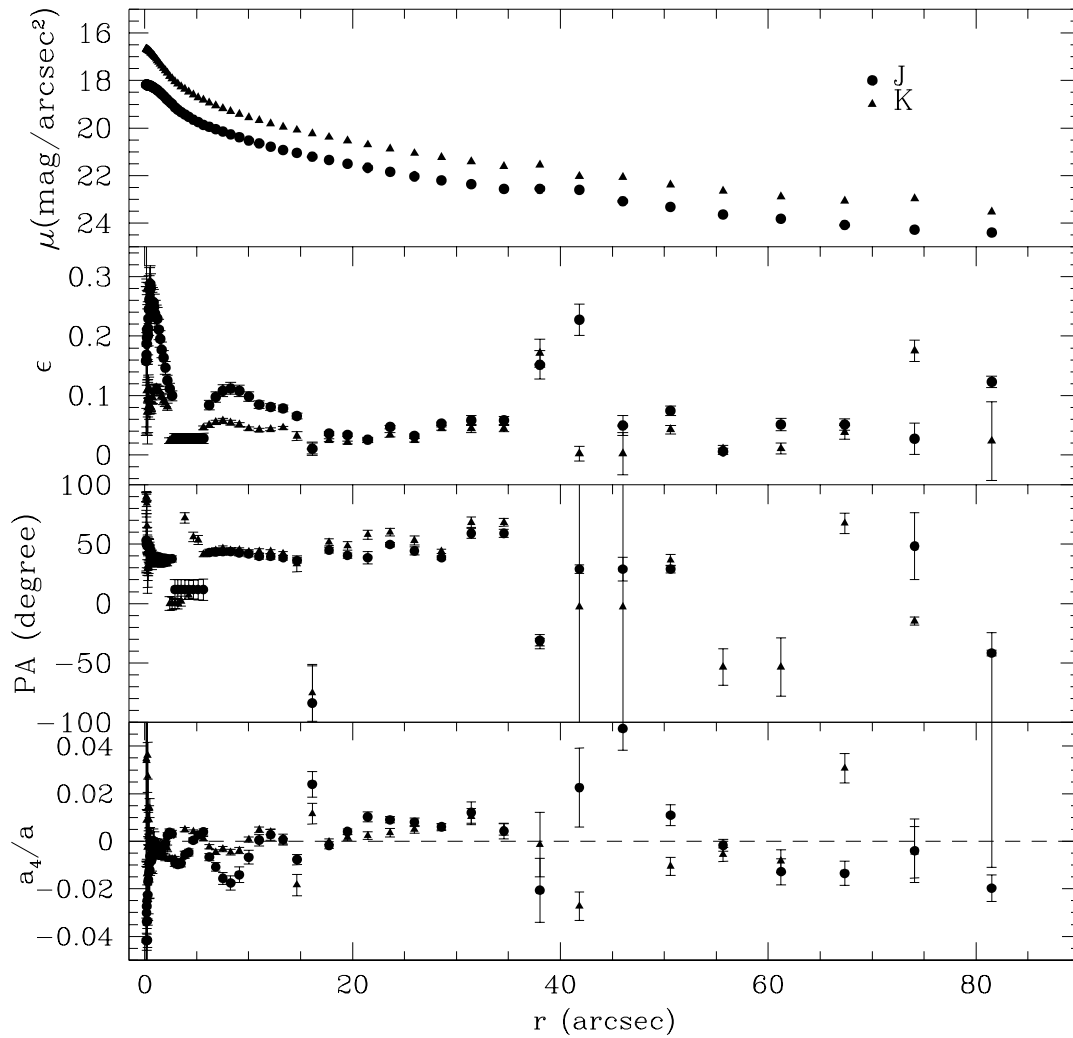


Figure 3. Ellipticity (ϵ), Position Angle (P.A.), mean surface brightness profile and shape parameter a_4/a in the J and K bands.

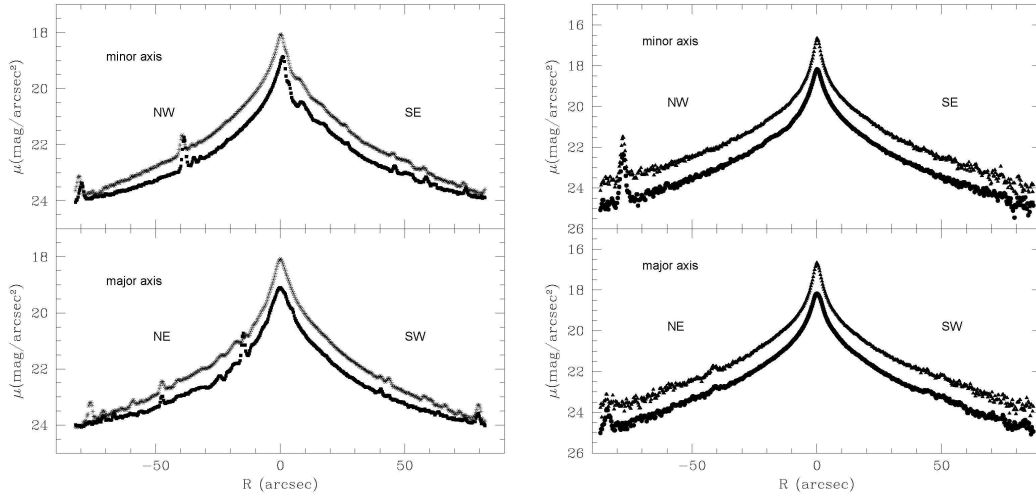


Figure 4. Light profiles along the minor (top-left panel) and major (bottom-left panel) axis of NGC1947 in the V (stars) and R band (triangles). Light profiles along the minor (top-right panel) and major (bottom-right panel) axis of NGC1947 in the J (stars) and K band (triangles)

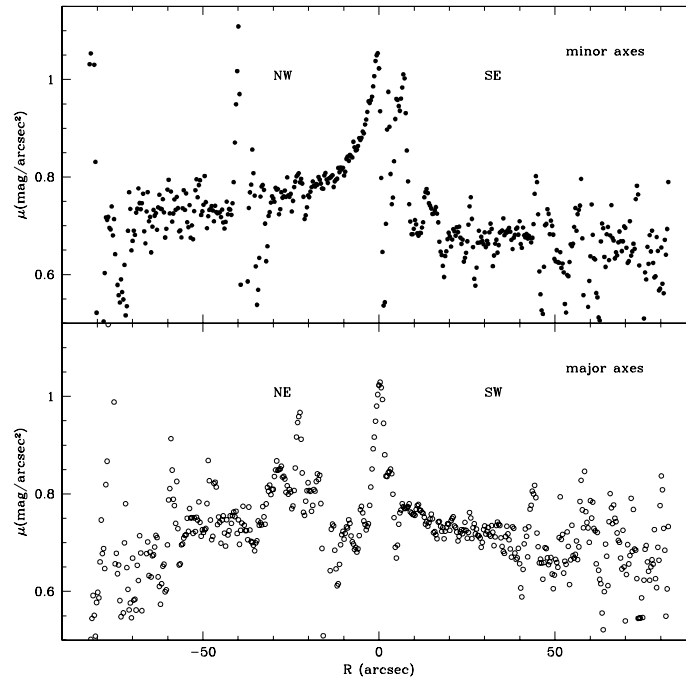


Figure 5. V-R color profiles along the minor (top panel) and major (bottom panel) axis of NGC1947.

Bekki K., 1998b, *ApJL*, 502, L133+

Bertola F., Bettoni D., Danziger J., Sadler E., Sparke L., de Zeeuw T., 1991, *ApJ*, 373, 369

Bertola F., Bettoni D., Rusconi L., Sedmak G., 1984, *AJ*, 89, 356

Bertola F., Galletta G., 1978, *ApJL*, 226, L115

Bertola F., Galletta G., Zeilinger W. W., 1992, *A&A*, 254, 89

Bettoni D., Galletta G., García-Burillo S., Rodríguez-Franco A., 2001, *A&A*, 374, 421

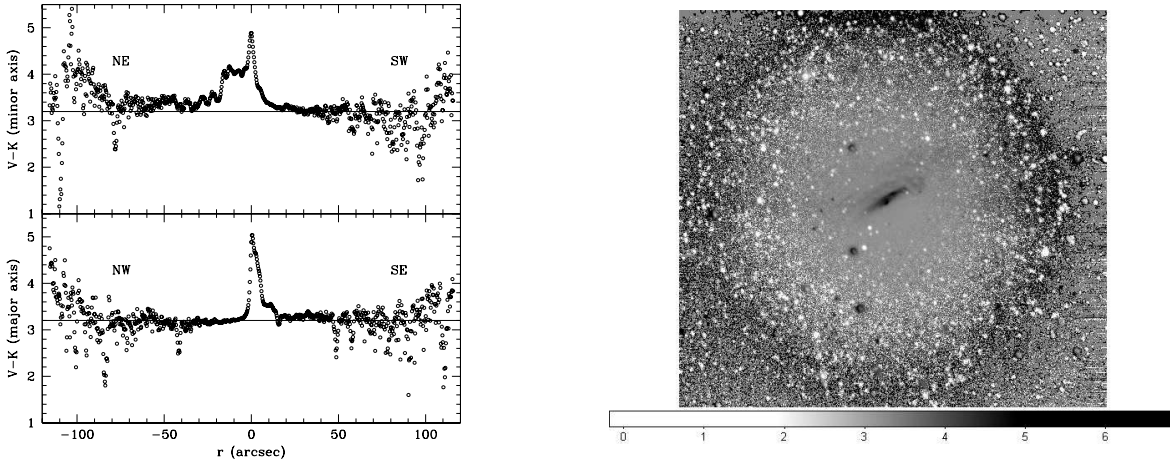


Figure 6. *Left panel* - V-K color profiles along the major (top panel) and minor (bottom panel) axis. The straight line correspond to the average V-K color for $r \geq 10$ arcsec. *Right panel* - V-K color map. The North is up, while the east is on the left of the image. Darker colors correspond to redder galaxy regions.

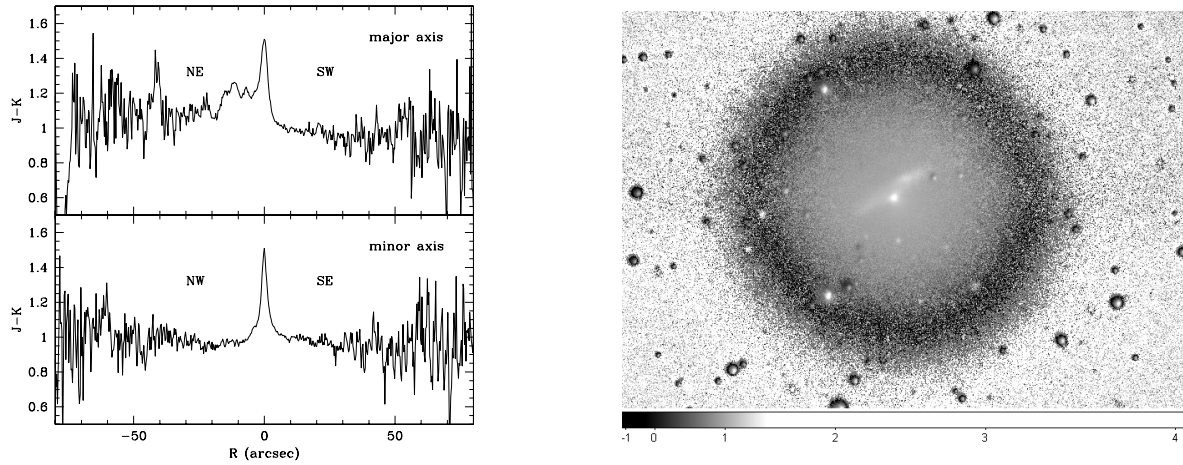


Figure 7. *Left panel* - J-K color profiles along the major (top panel) and minor (bottom panel) axis. *Right panel* - J-K color map. The North is up, while the east is on the left of the image. Lighter colors correspond to redder galaxy regions.

Bournaud F., Combes F., 2003, *A&A*, 401, 817

Bournaud F., Jog C. J., Combes F., 2005, *A&A*, 437, 69

Brocca C., Bettoni D., Galletta G., 1997, *A&A*, 326, 907

Brook C. B., Governato F., Quinn T., Wadsley J., Brooks A. M., Willman B., Stilp A., Jonsson P., 2008, *ArXiv e-prints*, 802

Bruzual G., Charlot S., 2003, *MNRAS*, 344, 1000

Bundy K., Fukugita M., Ellis R. S., Kodama T., Conselice C. J., 2004, *ApJL*, 601, L123

Carollo C. M., Danziger I. J., Buson L., 1993, *MNRAS*, 265, 553

Cole S., Lacey C. G., Baugh C. M., Frenk C. S., 2000, *MNRAS*, 319, 168

Conselice C. J., Bershadsky M. A., Dickinson M., Papovich C., 2003, *AJ*, 126, 1183

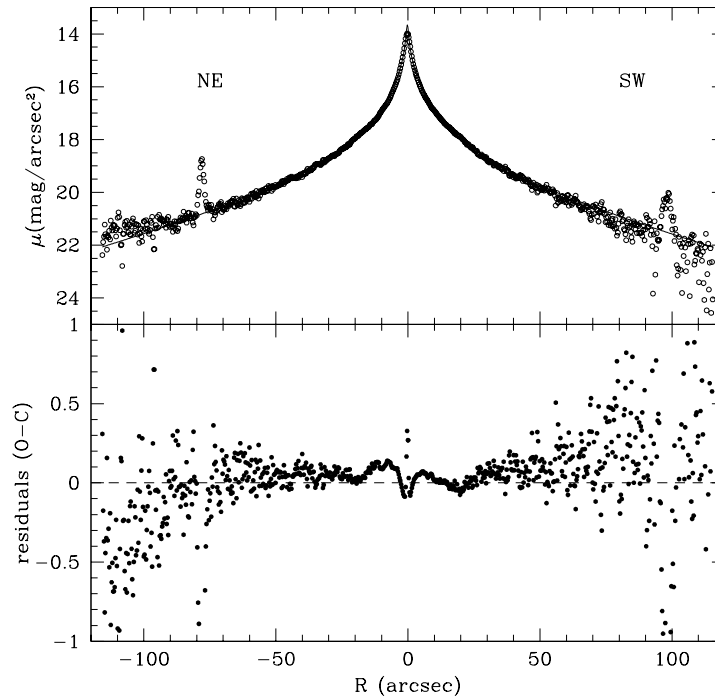


Figure 8. Top panel - 2-D fit of NGC1947 light distribution. The observed light profile along the major axis, is compared with those derived by the fit (continuous line). Bottom panel - Residuals between the observed and the fitted light profiles.

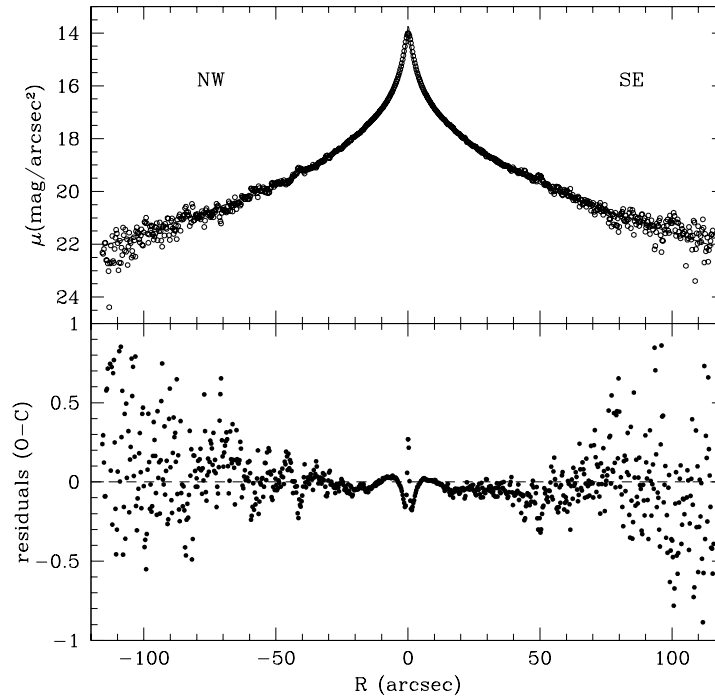


Figure 9. Top panel - 2-D fit of NGC1947 light distribution. The observed light profile along the minor axis, is compared with those derived by the fit (continuous line). Bottom panel - Residuals between the observed and the fitted light profiles.

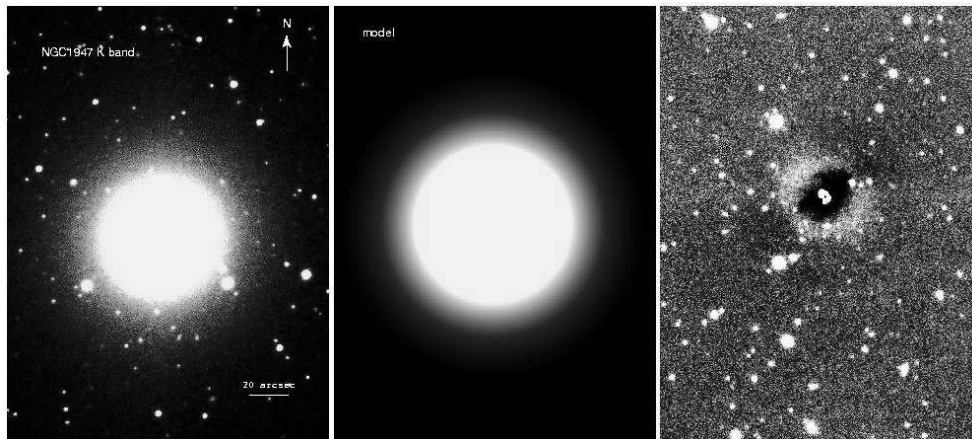


Figure 10. 2D fit of NGC1947. Left panel - K band image of NGC1947. Middle panel - Model of the galaxy. Right panel - Residual image.



Figure 11. Residuals of the subtraction of the K band model to the V band image.

Cox A. L., Sparke L. S., van Moorsel G., 2006, *AJ*, 131, 828

Davé R., Cen R., Ostriker J. P., Bryan G. L., Hernquist L., Katz N., Weinberg D. H., Norman M. L., O'Shea B., 2001, *ApJ*, 552, 473

De Propris R., Conselice C. J., Liske J., Driver S. P., Patton D. R., Graham A. W., Allen P. D., 2007, *ApJ*, 666, 212

de Vaucouleurs G., de Vaucouleurs A., Corwin H. G., 1976, 2nd reference catalogue of bright galaxies containing information on 4364 galaxies with reference to papers published between 1964 and 1975. University of Texas Monographs in Astronomy, Austin: University

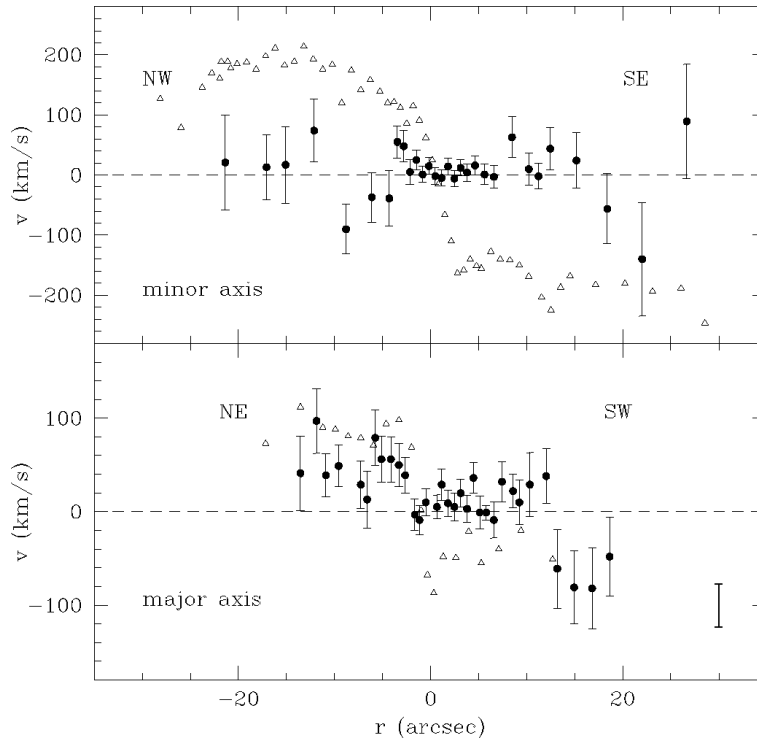


Figure 12. Stellar (filled points) and gaseous (triangles) rotation curves along the major (bottom panel) and minor axis (top panel) of NGC1947. The dashed line is the velocity of the galaxy center. In the bottom-right corner is plotted the error bar that represents the mean error on the velocity of the gas.

of Texas Press, 1976

Freeman K. C., 1970, *ApJ*, 160, 811

Galletta G., 1996, in Buta R., Crocker D. A., Elmegreen B. G., eds, *IAU Colloq. 157: Barred Galaxies Vol. 91 of Astronomical Society of the Pacific Conference Series, Counterrotation and Barred Galaxies*. pp 429–+

Galletta G., Sage L. J., Sparke L. S., 1997, *MNRAS*, 284, 773

Hawarden T. G., Longmore A. J., Tritton S. B., Elson R. A. W., Corwin Jr. H. G., 1981, *MNRAS*, 196, 747

Heisler J., Merritt D., Schwarzschild M., 1982, *ApJ*, 258, 490

Hernquist L., Weil M. L., 1993, *MNRAS*, 261, 804

Iodice E., Arnaboldi M., Sparke L. S., Buta R., Freeman K. C., Capaccioli M., 2004, *A&A*, 418, 41

Iodice E., Arnaboldi M., Sparke L. S., Freeman K. C., 2002, *A&A*, 391, 117

Iodice E., Arnaboldi M., Sparke L. S., Gallagher J. S., Freeman K. C., 2002, *A&A*, 391, 103

Kartalpepe J. S., Sanders D. B., Scoville N. Z., Calzetti D., Capak P., Koekemoer A., Mobasher B., Murayama T., Salvato M., Sasaki S. S., Taniguchi Y., 2007, *ApJS*, 172, 320

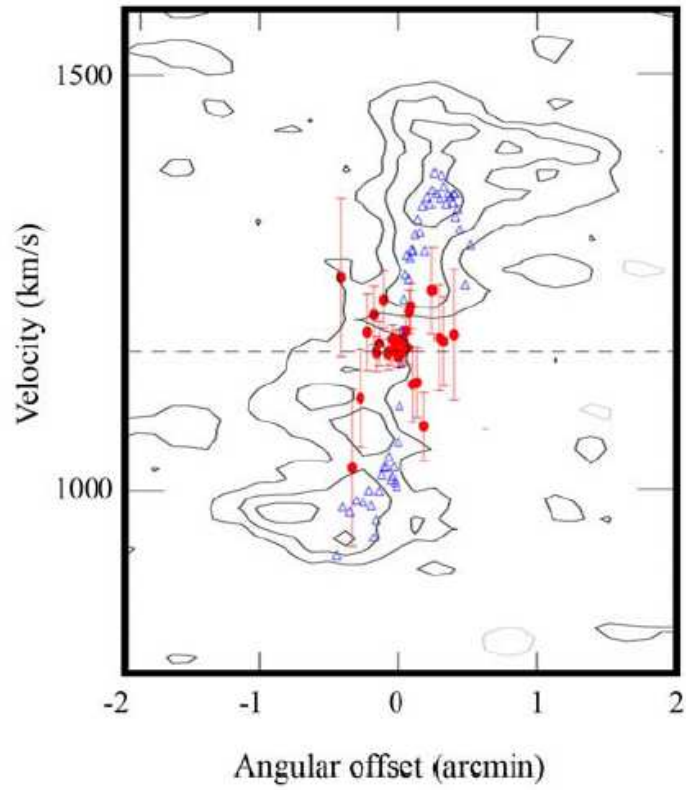


Figure 13. Stellar (filled points) and gaseous (triangles) rotation curves along the minor axis of NGC1947 superposed on the position-velocity plot of the HI along the $P.A. = 127^\circ$ presented by Oosterloo et al. (2002).

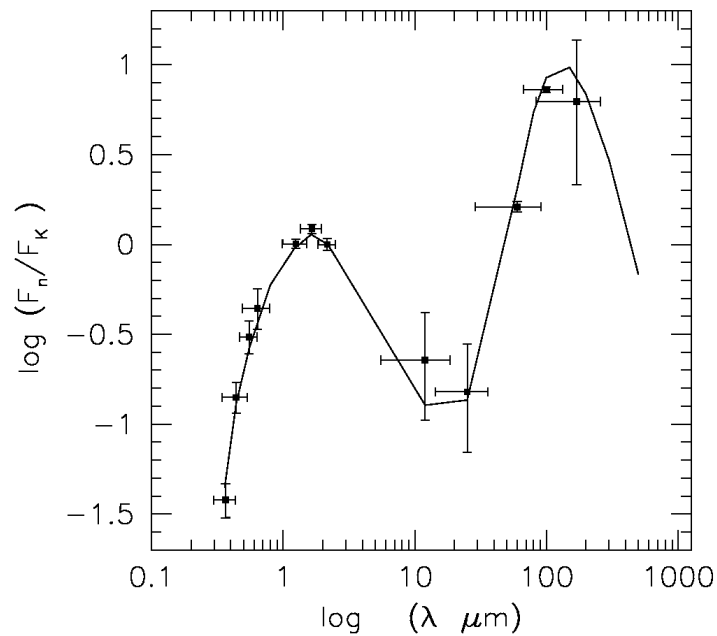


Figure 14. Continuous line shows the prediction of our model (see text); filled squares are V, J, and K integrated data given in sec. 3, the other data are from NED, in particular IRAS data at 12, 25, 60 100 μm and ISOPHOT data at 170 μm of Stickle et al. (2004).

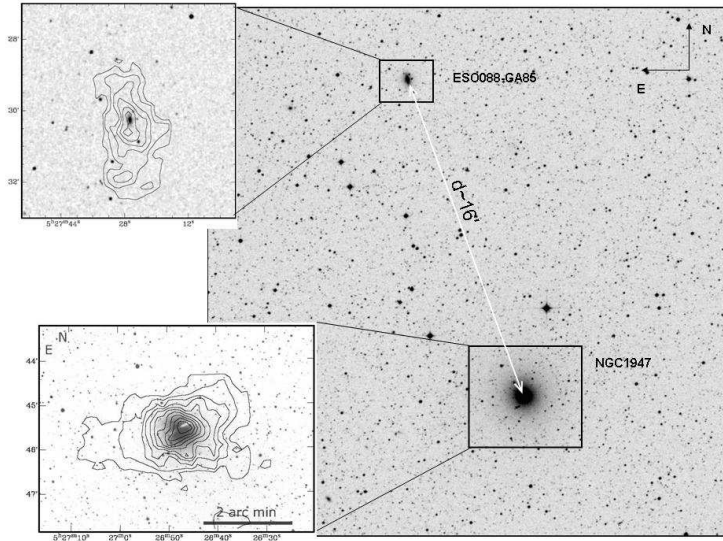


Figure 15. Image of a field of 25 arcmin around NGC1947. The two boxes on the left show the HI distribution for NGC1947 and ESO 085-GA088 published by Oosterloo et al. (2002).

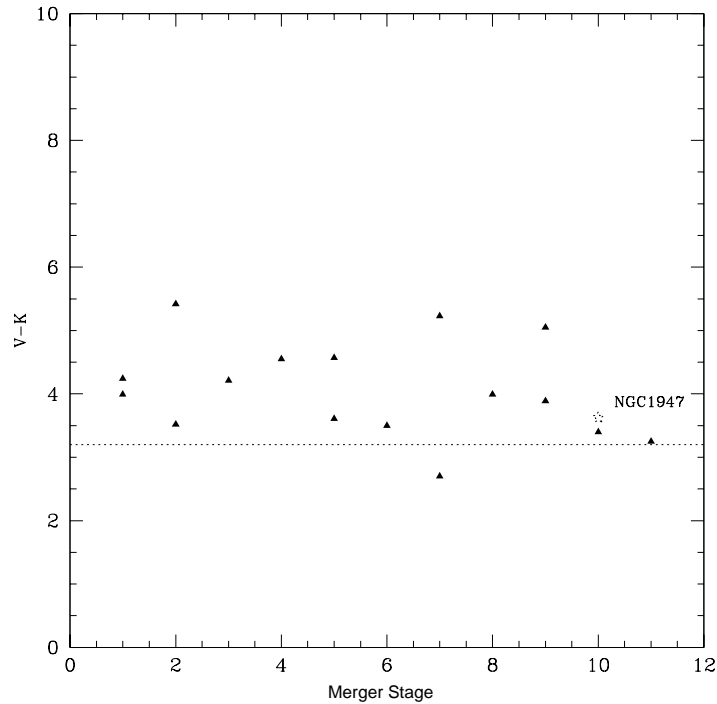


Figure 16. V-K color measured within 1kpc apertures as a function of the Toomre sequence merger stage. The dotted horizontal line indicates the V-K color for a SSP $10^{10}yr$ population of solar metallicity, which provides a reasonable fit to the measured colors for early-type galaxies.

Kereš D., Katz N., Weinberg D. H., Davé R., 2005, MNRAS, 363, 2

Lin L., Koo D. C., Willmer C. N. A., Patton D. R., Conselice C. J., Yan R., Coil A. L., Cooper M. C., Davis M., Faber S. M., Gerke B. F., Guhathakurta P., Newman J. A., 2004, ApJL, 617, L9

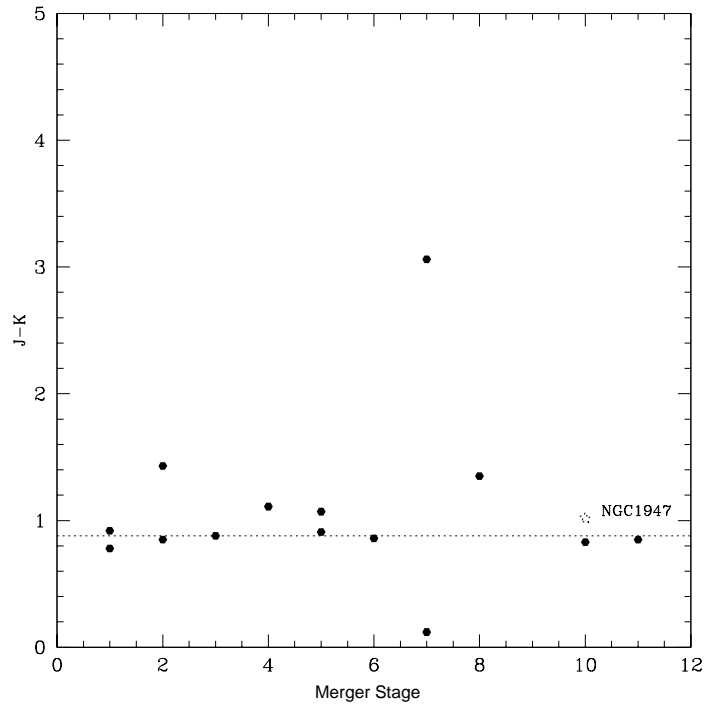


Figure 17. J-K color measured within 1kpc apertures as a function of the Toomre sequence merger stage. The dotted horizontal line indicates the J-K color for a SSP $10^{10}yr$ population of solar metallicity.

Lotz J. M., Davis M., Faber S. M., Guhathakurta P., Gwyn S., Huang J., Koo D. C., Le Floch E., Lin L., Newman J., Noeske K., Papovich C., Willmer C. N. A., Coil A., Conselice C. J., Cooper M., Hopkins A. M., Metevier A., Primack J., Rieke G., Weiner B. J., 2008, *ApJ*, 672, 177

Macciò A. V., Governato F., Horellou C., 2005, *MNRAS*, 359, 941

Malin D. F., Carter D., 1980, *Nature*, 285, 643

Mazzei P., Curir A., 2003, *ApJ*, 591, 784

Mazzei P., Curir A., Bonoli C., 1995, *AJ*, 110, 559

Mazzei P., Xu C., de Zotti G., 1992, *A&A*, 256, 45

Moellenhoff C., 1982, *A&A*, 108, 130

Oosterloo T. A., Morganti R., Sadler E. M., Vergani D., Caldwell N., 2002, *AJ*, 123, 729

Peng C. Y., Ho L. C., Impey C. D., Rix H.-W., 2002, *AJ*, 124, 266

Persson S. E., Murphy D. C., Krzeminski W., Roth M., Rieke M. J., 1998, *AJ*, 116, 2475

Quinn T., 1991, in Casertano S., Sackett P. D., Briggs F. H., eds, *Warped Disks and Inclined Rings around Galaxies Particle Simulations of Polar Rings*. pp 143–+

Reshetnikov V., Bournaud F., Combes F., Faúndez-Abans M., de Oliveira-Abans M., van Driel W., Schneider S. E., 2005, *A&A*, 431, 503

- Reshetnikov V., Sotnikova N., 1997, *A&A*, 325, 933
- Richter O.-G., Sackett P. D., Sparke L. S., 1994, *AJ*, 107, 99
- Rossa J., Laine S., van der Marel R. P., Mihos J. C., Hibbard J. E., Böker T., Zabludoff A. I., 2007, *AJ*, 134, 2124
- Sage L. J., Galletta G., 1993, *ApJ*, 419, 544
- Salpeter E. E., 1955, *ApJ*, 121, 161
- Sandage A., Tammann G. A., 1987, *A revised Shapley-Ames Catalog of bright galaxies*. Carnegie Institution of Washington Publication, Washington: Carnegie Institution, 1987, 2nd ed.
- Sargent W. L. W., Schechter P. L., Boksenberg A., Shortridge K., 1977, *ApJ*, 212, 326
- Schinnerer E., Scoville N., 2002, *ApJL*, 577, L103
- Semelin B., Combes F., 2005, *A&A*, 441, 55
- Serra P., Trager S. C., Oosterloo T. A., Morganti R., 2007, *ArXiv e-prints*, 712
- Sersic J. L., 1968, *Atlas de galaxias australes*. Cordoba, Argentina: Observatorio Astronomico, 1968
- Stickel M., Lemke D., Klaas U., Krause O., Egner S., 2004, *A&A*, 422, 39
- Thakar A. R., Ryden B. S., 1996, *ApJ*, 461, 55
- Thakar A. R., Ryden B. S., 1998, *ApJ*, 506, 93
- Toomre A., 1977, in Tinsley B. M., Larson R. B., eds, *Evolution of Galaxies and Stellar Populations Mergers and Some Consequences*. pp 401–+
- Toomre A., Toomre J., 1972, *ApJ*, 178, 623
- van Driel W., Combes F., Arnaboldi M., Sparke L. S., 2002, *A&A*, 386, 140

This paper has been typeset from a \TeX / \LaTeX file prepared by the author.